# In-plane anisotropy of the photon-helicity induced linear Hall effect in few-layer WTe_{2}

Paul Seifert, Florian Sigger, Jonas Kiemle, Kenji Watanabe, Takashi Taniguchi, Christoph Kastl, Ursula Wurstbauer, and Alexander Holleitner

Phys. Rev. B **99**, 161403 — Published 11 April 2019

DOI: 10.1103/PhysRevB.99.161403

# In-plane anisotropy of the photon-helicity induced linear Hall effect in few-layer $WTe_2$

Paul Seifert[1], Florian Sigger[1,2], Jonas Kiemle[1], Kenji Watanabe[3], Takashi Taniguchi[3], Christoph Kastl[4], Ursula Wurstbauer[1,2,5] and Alexander Holleitner[1,2]

*1 Walter Schottky Institut and Physics Department, Technical University of Munich, Am Coulombwall 4a, 85748 Garching, Germany.*

*2 Nanosystems Initiative Munich (NIM), Schellingstr. 4, 80799 Mnchen, Germany.*

*3 Advanced Materials Laboratory, National Institute for Materials Science, Tsukuba, Ibaraki 305-0044, Japan.*

*4 Molecular Foundry, Lawrence Berkeley National Laboratory, One Cyclotron Road, 94720 Berkeley, California, United States.*

*5 Institute of Physics, University of Mnster, Wilhelm-Klemm-Str. 10, 48149 Mnster, Germany*

(Dated: Oktober 1, 2018)

Using Hall photovoltage measurements, we demonstrate that a linear transverse Hall-voltage can be induced in few layer $WTe_2$ under circularly polarized light illumination. By applying a bias voltage along different crystal axes, we find that the photon-helicity induced Hall effect coincides with a particular crystal axis. Our results are consistent with the underlying Berry-curvature exhibiting a dipolar distribution due to the breaking of crystal inversion symmetry. Using a time-resolved optoelectronic auto-correlation spectroscopy, we find that the decay time of the detected Hall voltage exceeds the electron-phonon scattering time by orders of magnitude but is consistent with the comparatively long spin-lifetime of carriers in the momentum-indirect electron and hole pockets in $WTe_2$. Our observation suggests, that a helicity induced non-equilibrium spin density on the Fermi surface after the initial charge carrier relaxation gives rise to a linear Hall effect.

## INTRODUCTION

In recent years, materials that exhibit a non-trivial topological band-structure and non-zero Berry-curvature have attracted a lot of attention. These properties render the materials a very promising and robust platform for spintronic applications independent of the exact details of material composition or extrinsic influences such as temperature. The Berry-curvature describes the local self-rotation of a quantum wave-packet and can effectively act as a magnetic field largely impacting the electronic properties of a system [1]. The Berry-curvature affects the Hall-conductivity and spin-Hall conductivity, which is the antisymmetric non-dissipative addition to the Ohmic conductivity in the absence of time-reversal symmetry or crystal inversion symmetry, respectively [2]. In this context, $WTe_2$ a layered van-der-Waals material, became the subject of extensive research. Monolayer $WTe_2$ was demonstrated to host both a topologically non-trivial quantum spin-Hall gap [3–5], as well as a Berry curvature dipole that leads to the so-called circular photogalvanic effect when inversion symmetry is broken via an out-of-plane electric field [6]. Bulk $WTe_2$ is known as the prototypical type-II Weyl semimetal, a material shown to exhibit chiral Weyl-fermions at the surface that break Lorentz-invariance [7]. In particular, the Weyl points, which are linear band-crossing points in Weyl semimetals, represent monopoles of Berry curvature and come pairwise with opposite chirality [8]. It is proposed, that under circularly polarized (CP) illumination, a momentum-shift of the Weyl-points gives rise to a photoinduced anomalous Hall effect during optical excitation [9]. Moreover, $WTe_2$ exhibits the highest values of a non-saturating magnetoresistance ever reported [10].

In contrast to monolayer $WTe_2$, inversion symmetry is intrinsically broken in few-layered and bulk $WTe_2$ [11]. This renders few layer $WTe_2$ a promising candidate to host non-trivial spin-transport phenomena, as a non-zero Berry curvature on the non-equilibrium Fermi surface is predicted [12]. The Berry curvature directly impacts the electronic transport properties of a material. In the presence of an electric field, an electron with eigenenergy $\epsilon_n(\mathbf{k})$ occupying a specific band $n$ can pick up an additional transverse velocity contribution, which is proportional to the Berry curvature $\Omega_n(\mathbf{k})$ of the specific band [1],

$$v_n(\mathbf{k}) = \frac{\delta\epsilon_n(\mathbf{k})}{\hbar\delta\mathbf{k}} - \frac{e}{\hbar}\mathbf{E}\times\Omega_n(\mathbf{k}), \tag{1}$$

where the second term is the transverse velocity contribution. It is always transverse to the electric field and is responsible for various Hall effects [1]. The Berry curvature $\Omega_n(\mathbf{k})$ is directly related to the symmetry of the system's Hamiltonian. An electron's velocity must be unchanged undergoing symmetry operations that reflect the symmetries of the unperturbed system. Accordingly, eq. 1 dictates that $\Omega_n(\mathbf{k}) = -\Omega_n(-\mathbf{k})$ if the system is invariant under time-reversal and $\Omega_n(\mathbf{k}) = \Omega_n(-\mathbf{k})$ if the system is invariant under spatial inversion [1]. If time-reversal symmetry is broken, a net $\Omega_n$ can occur when integrating across the Brillouin-zone leading to a net Hall conductivity and a corresponding Hall voltage under applied bias. If inversion symmetry is broken, time-reversal dictates, that the net $\Omega_n$ is zero, when integrating across the Brillouin-zone, but it can exhibit a dipolar structure where opposite points in $k$-space exhibit opposite $\Omega_n(\mathbf{k})$ and opposite transverse velocities [1, 13, 14]. Hence the intrinsic breaking of spatial inversion symmetry promises few layer $WTe_2$ to host non-trivial Berry curvature re-

lated transport phenomena on the Fermi surface such as the non-linear Hall effect [15, 16].
In the present work, we explore the transverse conductivity in few layer $WTe_2$ under electrical current flow using polarization- and time-resolved photoexcitation at room temperature. We detect a finite photoinduced transverse voltage that switches sign with the polarity of the applied longitudinal current as well as with the helicity of the excitation laser. The helicity dependent transverse conductivity only occurs when the current is injected orthogonal to the crystal's mirror-plane. This observation suggests the intrinsic breaking of inversion symmetry with a respective dipolar structure of the Berry curvature as the underlying physics [14, 17]. We further reveal a characteristic lifetime of the transverse conductivity of $> 100$ ps exceeding the reported carrier-phonon scattering time by orders of magnitude [18]. Therefore, the lifetime of the observed transverse voltage is associated with the reported spin-lifetime of carriers in the momentum-indirect electron and hole pockets in $WTe_2$ [18, 19]. Our observation suggests, that a helicity induced non-equilibrium spin density on the Fermi surface is the underlying mechanism of the linear Hall effect after the initial charge carrier relaxation has taken place.

We exfoliate individual few-layer flakes of the type-II Weyl-semimetal $WTe_2$ (HQ Graphene) onto a transparent sapphire substrate with pre-fabricated Ti/Au contacts in a four-terminal geometry. We focus a circularly polarized laser with a photon energy of 1.5 eV onto the centre of the flake. To avoid degradation effects and to maintain a high device quality, the $WTe_2$-flakes are encapsulated with a thin crystal of high quality hexagonal boron nitride (hBN) [21, 22]. Figure 1(a) sketches our measurement geometry of the photo-induced linear Hall effect. A bias voltage is applied between the source and drain contacts and it drives a current **j**. A high impedance differential voltage amplifier is wired to the two remaining contacts in perpendicular direction for the measurement of the photo-induced transverse voltage $V^{\mathrm{photo}}$. The excitation with circularly polarized light induces a net spin density on the non-equilibrium Fermi surface, which breaks time-reversal symmetry and gives rise to a corresponding Hall conductivity $\sigma_H$. Under current flow, the Hall conductivity $\sigma_H$ can be detected as a net transverse Hall voltage orthogonal to the light propagation and the source-drain current density **j**. Figure 1(b) shows a microscope image of a four-terminal $WTe_2$/h-BN device and the electrical circuitry. The distance between the contacts of 14 µm is chosen to be much larger than the size of our laser spot of $\approx 1.5$ µm in order to exclude extrinsic effects that stem from an illumination of the metal contacts or crystal boundaries [6]. Figures 1(c) and (d) sketch the side- and top-view of the layered crystal structure of $WTe_2$. In contrast to most TMDs, which exhibit a hexagonal structure with space-group $D_{6h}$, bulk $WTe_2$ crystallizes in an orthorhombic phase with space group $C_{2v}$ featuring a single mirror plane $M_a$ orthogonal to the a-axis. In the $T_d$-phase, atoms in neighbouring layers are rotated by a spatial angle of $\pi$ with respect to each other, which breaks inversion symmetry along the b-axis and leads to a dipolar structure of the Berry-curvature [4, 11, 23, 24]. Due to the different dielectric environment above (h-BN) and below ($Al_2O_3$) the $WTe_2$ flake, we also cannot exclude a weak breaking of inversion-symmetry along the c-direction of the crystal.

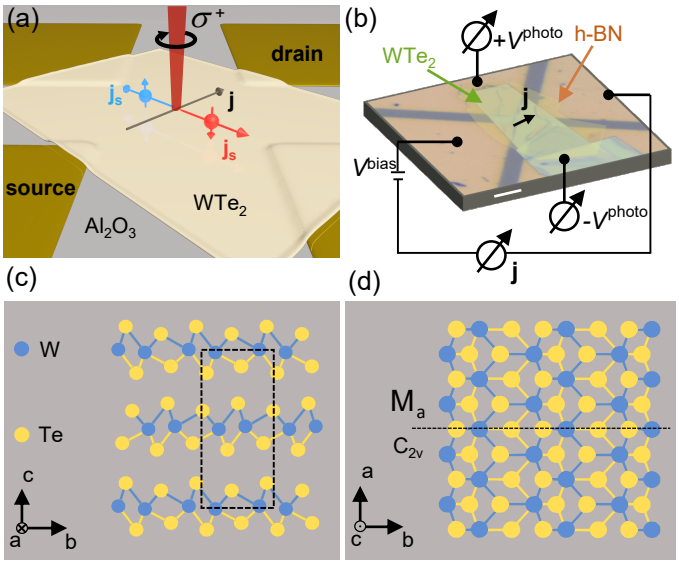


FIG. 1. (a) Schematic of a linear Hall effect driven by a net spin polarization induced by illumination with circularly polaried light. Red and blue spheres represent opposite spin polarizations flowing perpendicular to a current **j**. A photo induced, out-of-equillibrium spin density leads to a net Hall photovoltage via the breaking of time-reversal symmetry. (b) Optical microscope image and experimental circuitry of a four-terminal device of $WTe_2$ encapsulated in h-BN. Scale bar is 10 µm. (c) Side view on the crystal structure of few-layer $T_d$-phase $WTe_2$ where a and b denote the in-plane and c the out-of-plane crystal axis directions. In the $T_d$-phase, inversion symmetry is broken along the b-axis. (d) Top view of the crystal structure of $T_d$-$WTe_2$. The crystal exhibits a mirror plane $M_a$ orthogonal to the a-axis.

Figure 2 presents polarization-resolved transverse photovoltage measurements. The laser is focused at the center of the $WTe_2$ flake and a bias voltage $V_{1-3}^{\mathrm{bias}}$ is applied between source (1) and drain (3), while the photovoltage $V_{2-4}^{\mathrm{photo}}$ is measured between (2) and (4) [Fig 2 (a)]. The laser polarization is modulated with a quarter-wave plate. Figures 2(b) and (c) show the polarization dependent transverse voltage $V_{2-4}^{\mathrm{photo}}$ for bias voltages of $V_{1-3}^{\mathrm{bias}} = +\ 0.4$ V and $V_{1-3}^{\mathrm{bias}} = -\ 0.4$ V, respectively. A clear transverse $V_{2-4}^{\mathrm{photo}}$ is detectable and can be modulated with the laser helicity. Figure 2 (d) shows selectively the helicity dependent photovoltage

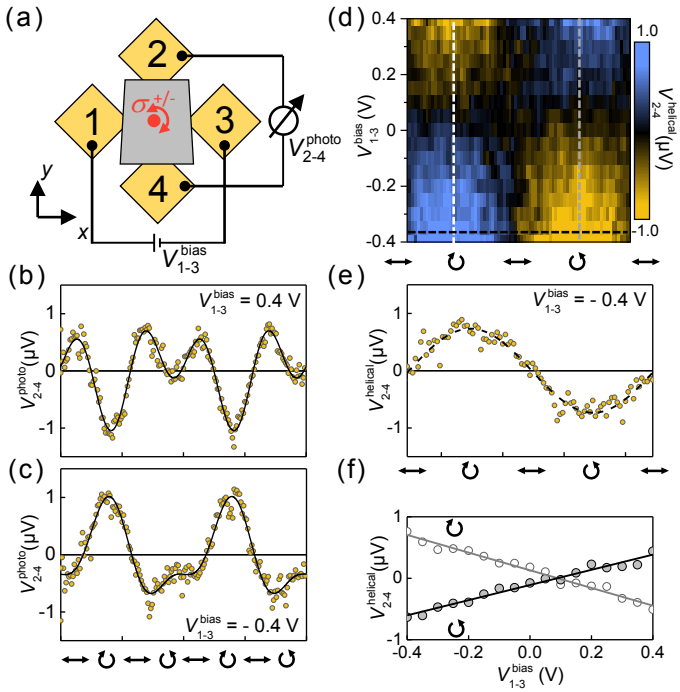


FIG. 2. Polarization-resolved transverse photovoltage measurements. (a) Schematic of the measurement geometry. The source-drain bias $V_{1-3}$ is applied between the contacts labelled (1) and (3). The transverse voltage $V_{2-4}$ is measured between the contacts labelled (2) and (4). All measurements are conducted at room temperature. (b) and (c) Polarization dependence of the transverse photovoltage $V^{photo}_{2-4}$, for applied bias voltages of $V^{bias}_{1-3}$ = 0.4 V and $V^{bias}_{1-3}$ = -0.4 V, respectively. The photoresponse is dominated by the photon helicity and the polarization dependence switches polarity with the applied bias $V^{bias}_{1-3}$. (d) Bias dependence of the helicity dependent photovoltage $V^{helical}_{2-4}$. The modulation with the linear polarization is subtracted via a fit procedure (compare supplementary Figs. S1 and S2 [20]). (e) $V^{helical}_{2-4}$ along the black dashed line in (d). (f) Source-drain bias dependence of $V^{helical}_{2-4}$ for circularly right and left polarized light, along the grey and white dashed lines in (d).

contribution $V^{helical}_{2-4}$ as a function of bias voltages $V^{bias}_{1-3}$ and laser polarization. The helicity independent contributions are subtracted via a fit procedure according to their characteristic frequency with the angle of the quarter-wave plate (compare supplementary Figs. S1 and S2 [20]) [25]. Line-cuts through the helical photovoltage map [Fig. 2(d)] are drawn in Fig. 2(e) along the polarization axis and Fig. 2(f) along the bias axis for different laser helicities. The transverse photovoltage $V^{helical}_{2-4}$ changes polarity with the laser helicity and depends linearly on the longitudinal bias-voltage $V^{bias}_{1-3}$. In principle a circular photo-galvanic effect can also contribute to the current signal as a bias-independent off-set to our signal [6, 15]. In other words, the off-set in the longitudinal bias in Fig. 2 (f) might resemble the circular photo-galvanic effect.

In order to determine how the transverse photovoltage

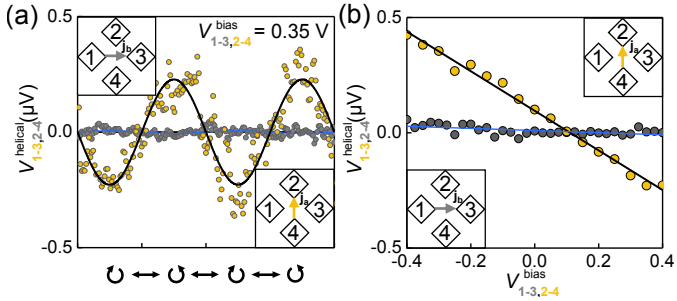


FIG. 3. Crystal axis dependent photovoltage. (a) Comparison of the transverse helicity dependent $V^{helical}$ induced in the sample for a bias $V^{bias}$ applied along the crystal axes orthogonal (yellow, 2-4) and parallel (grey, 1-3) to the crystals mirror plane $M_a$. (b) Amplitude of $V^{helical}$ vs. the applied bias $V^{bias}$ along the two different crystal axes. Respective measurement configurations are indicated by the insets in accordance with the geometry in Fig. 2 (a).

depends on the crystal axis, we perform measurements on a sample, where the crystal axes are aligned to the measurement axes of our four-terminal contact geometry during sample fabrication. The $x$-axis [$y$-axis, compare Fig. 2 (a)] of our measurement geometry coincides with the b-axis (a-axis) of this $WTe_2$ crystal as determined by polarization resolved Raman spectroscopy (supplementary Fig. S3 [20]) [26]. Figure 3 (a) shows the helicity dependent transverse photovoltage for a bias applied between contacts (1) and (3) (b-axis, grey dots) and between contacts (2) and (4) (a-axis, yellow dots). For a bias applied along the b-axis, no distinct helicity dependent transverse photovoltage is visible. For a bias applied along the a-axis, a transverse photovoltage emerges for CP illumination. Figure 3 (b) shows the amplitude of the helicity dependent transverse photovoltage $V^{helical}$ vs bias voltage $V^{bias}$ applied along the respective crystal directions. We find a finite $V^{helical}$, which depends linearly on the longitudinal bias if the bias is applied along the a-axis (yellow). In contrast, we detect no significant $V^{helical}$ when the bias is applied along the b-axis (grey).

In a next step, we perform time-resolved auto-correlation measurements to extract the characteristic time scales of the involved processes. Figure 4 (a) shows a schematic of our measurement geometry. A 150 fs pump pulse at a photon energy of 1.5 eV excites the center of the sample from the top at a fixed laser helicity. A probe pulse with identical duration and energy but variable helicity is delayed via a mechanical delay-stage and focused onto the same spot from the backside. Both pump and probe lasers are modulated at different frequencies, and the auto-correlation signal of the transverse photovoltage is detected at the sum-frequency with a lock-in amplifier. Figure 4 (b) shows the time-resolved difference of the transverse photovoltage for co-polarized and cross-polarized pump/probe excitation. We observe a finite difference directly after the excitation, which

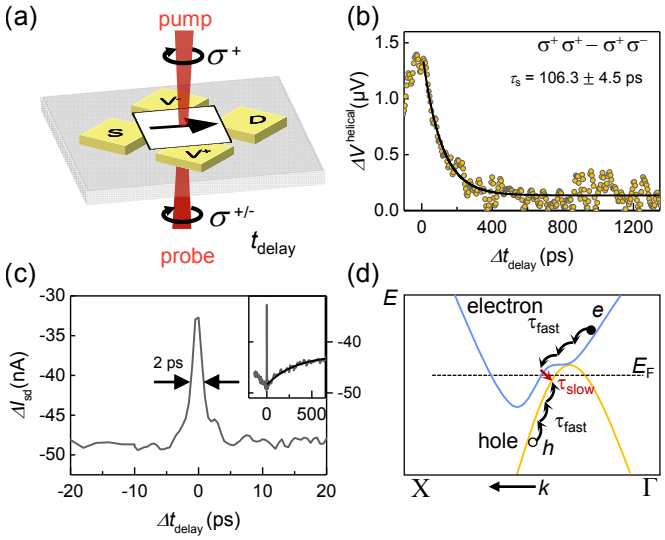


FIG. 4. Time-resolved optoelectronic auto-correlation of spin and charge dynamics. (a) Schematic illustrations for measuring the auto-correlation of the helicity dependent transverse photovoltage. (b) Difference between co-polarized and cross-polarized probe laser excitation as a function of time delay. (c) Time-resolved pump/probe auto-correlation measurements of the longitudinal source-drain current with applied bias. The inset displays the same measurement on a longer time-scale. (d) Schematic band structure of $WTe_2$ near the Fermi level ($E_F$) along the Γ -X direction. The fast relaxation time $\tau_{fast}$ describes the electron-phonon thermalization process and $\tau_{slow}$ represents the phonon-assisted interband e-h recombination process.

decays exponentially on a timescale of $\tau_{slow} \approx 106.3 \pm 4.5$ ps. We interpret the difference between co-polarized and cross-polarized auto-correlation of the transverse photovoltage as a signature of the photo-excited spin population. Intriguingly, the decay time surpasses the electron-phonon relaxation time of a few ps by orders of magnitude [18, 27]. In fact, the slow time-scale $\tau_{slow}$ of spin relaxation was reported to be limited by the phonon-assisted recombination of momentum indirect electron-hole pairs, suggesting, that the charge carrier-relaxation to the Fermi-energy does not significantly randomize the spin-polarization [19]. We note that we determine a transport time, which reflects a large momentum excitation, whereas ref. [19] reports on excitations with vanishingly small momentum values. The difference between $\tau_{slow}$ and the nanosecond lifetime in [19] might be further explained by the specific dielectric environment of the hBN ($SiO_2$) top (bottom) layer. Figure 4 (c) shows the time-resolved auto-correlation of the longitudinal photo-current measured in the direction between the source and drain contacts. In contrast to the transverse photovoltage, the main time-scale dominating the longitudinal photocurrent, which we denote as $\tau_{fast}$ is in the order of 2 ps and can be interpreted as an instantaneous photo-conductance increase, which is limited by the phonon-mediated charge carrier-relaxation to the Fermi-energy [18, 19, 27]. We note, that a slower time-scale is also detectable in the photo-current to a lesser extent. This indicates that the charge carrier spin does also impact the longitudinal charge transport, e.g. by anisotropic optical absorption as a consequence of a chiral anomaly in Weyl-semimetals [28–30]. Figure 4(d) shows a schematic energy band-diagram of the electron and hole pockets along the $\Gamma - X$ direction. The phonon-mediated carrier relaxation and recombination channels are indicated by their characteristic time-scales $\tau_{fast}$ and $\tau_{slow}$, respectively.

*Discussion* According to equation (1), the Berry-curvature must vanish in systems, which have both inversion- and time-reversal symmetry. The intrinsic breaking of the bulk inversion symmetry in $WTe_2$ along one crystal axis is predicted to induce a dipolar Berry curvature [13]. Phenomenologically, the anisotropic Berry curvature is consistent with the crystal axis dependence of our measured transverse photovoltage. We find a linearly bias dependent transverse photovoltage $V^{helical}$ only if the bias is applied along the a-axis orthogonal to the mirror-plane $M_a$. The bias-dependence clearly demonstrates that the observed $V^{helical}$ is not caused by a local photo-voltage generation e.g. due to built-in fields or impurities, but it is intrinsic in nature and proportional to the applied external electric field [25]. The transverse photovoltage switches polarity with the helicity of the exciting laser, which establishes that the underlying origin of the transverse conductivity is either directly based on the photon chirality [9] or on the corresponding excited spin-density in the $WTe_2$ [25, 31, 32]. As we detect $V^{helical}$ on a long characteristic time scale $\approx 100$ ps, although the laser pulse duration is only 150 fs, we identify the transverse photovoltage to stem from the excited non-equilibrium spin-density on the Fermi surface after the initial charge carrier relaxation, rather than from a laser field driven anomalous Hall conductivity as suggested for a CW-laser excitation [9]. In our point of view, the 2 ps-relaxation time of the longitudinal current [Fig. 4 (c)] is a clear indication that the photo-excited charge carriers give rise to a non-equilibrium spin- and charge carrier ensemble at the Fermi surface. In turn, the transverse voltage component with 100 ps time constant probes the properties of the Fermi surface. Experimentally, we can only detect the Hall voltage and its lifetime, but we cannot directly resolve the spin-polarization of the charge carriers giving rise to this transverse conductivity. Likewise time-resolved magneto-optical Kerr spectroscopy as in ref [19] can only indicate a long spin relaxation time but not a spin-transport. In turn, we cannot distinguish a linear Hall effect which is induced by a non-equilibrium spin density on the Fermi surface, from an anomalous Hall effect induced by the same non-equilibrium spin density. In both cases, however, the underlying Hamiltonian is not invariant under time reversal, and in turn, it allows

for a finite Hall voltage under applied bias. In principle, charge carriers can also acquire a transverse velocity from extrinsic mechanisms such as skew-scattering and side-jump contributions, which can also be proportional to the Berry-curvature [33, 34]. Experimentally, we generate the signal locally within the laser spot ($\approx 1.5$ μm) and detect the photovoltage at rather macroscopic distances of 14 μm. In metallic systems such as $WTe_2$ the detection occurs instantaneously according to the so-called Shockley-Ramo theorem [35]. Therefore, we cannot distinguish between intrinsic Berry-phase effects and the extrinsic contributions, which are proportional to the Berry curvature. With the observed anisotropy, however, we can exclude extrinsic contributions, which do not depend on the crystal axis and in turn, on the Berry curvature [34, 36]. Rationalized by this microscopic model, we interpret the transverse conductivity to stem from a laser-helicity induced non-equilibrium spin-ensemble after the initial carrier relaxation. In contrast to the case of topological insulators, such as $Bi_2Te_2Se$ [25, 31, 32] where a longitudinal edge photoconductance is suggested to originate from an isotropic photo induced spin-Hall effect [25], the described anisotropic helicity induced linear Hall effect is deeply rooted within the intrinsic bulk crystal symmetries of few layer $WTe_2$. The corresponding anisotropy also distinguishes the here reported effect from the isotropic photo-induced anomalous Hall effect in spin-orbit coupled materials with a dominating Rashba term such as GaN [37]

*Conclusion* We explore the transverse conductivity in few layer $WTe_2$ under illumination and electrical current flow using polarization and time-resolved transverse photovoltage measurements. Our findings suggest that a helicity induced non-equilibrium spin density on the Fermi surface gives rise to an unprecedented anisotropic linear Hall effect after the initial carrier relaxation. The results are consistent with the underlying Berry-curvature exhibiting a dipolar distribution on the Fermi surface. We further reveal, that the characteristic decay-time of the transverse Hall-voltage exceeds the carrier-phonon scattering time by orders of magnitude but is consistent with the spin-lifetime of carriers in the momentum-indirect electron and hole pockets in $WTe_2$.

*Acknowledgements* We thank T. Schmidt and M. Burghard for discussions. This work was supported by the DFG via SPP 1666 (grant HO 3324/8) and the Munich Center for Quantum Science and Technology (MCQST) EXC-2111 390814868. C. K. acknowledges funding by the Molecular Foundry supported by the Office of Science, Office of Basic Energy Sciences, of the US Department of Energy under Contract No. DE-AC02-05CH11231.

In the course of the review process, we became aware of related work on a photoinduced Hall effect in graphene [38].

## REFERENCES

[1] D. Xiao, M. C. Chang, and Q. Niu, Rev. Mod. Phys. **82**, 1959 (2010).
[2] F. D. M. Haldane, Phys. Rev. Lett. **93**, 206602 (2004).
[3] Z. Fei, T. Palomaki, S. Wu, W. Zhao, X. Cai, B. Sun, P. Nguyen, J. Finney, X. Xu, and D. H. Cobden, Nat. Phys. **13**, 677 (2017).
[4] S. Tang, C. Zhang, D. Wong, Z. Pedramrazi, H. Z. Tsai, C. Jia, B. Moritz, M. Claassen, H. Ryu, S. Kahn, J. Jiang, H. Yan, M. Hashimoto, D. Lu, R. G. Moore, C. C. C. Hwang, C. C. C. Hwang, Z. Hussain, Y. Chen, M. M. Ugeda, Z. Liu, X. Xie, T. P. Devereaux, M. F. Crommie, S. K. Mo, and Z. X. Shen, Nat. Phys. **13**, 683 (2017).
[5] S. Wu, V. Fatemi, Q. D. Gibson, K. Watanabe, T. Taniguchi, R. J. Cava, and P. Jarillo-Herrero, Science **359**, 76 (2018).
[6] S. Y. Xu, Q. Ma, H. Shen, V. Fatemi, S. Wu, T. R. Chang, G. Chang, A. M. Valdivia, C. K. Chan, Q. D. Gibson, J. Zhou, Z. Liu, K. Watanabe, T. Taniguchi, H. Lin, R. J. Cava, L. Fu, N. Gedik, and P. Jarillo-Herrero, Nat. Phys. **14**, 900 (2018).
[7] A. A. Soluyanov, D. Gresch, Z. Wang, Q. Wu, M. Troyer, X. Dai, and B. A. Bernevig, Nature **527**, 495 (2015).
[8] X. Wan, A. M. Turner, A. Vishwanath, and S. Y. Savrasov, Phys. Rev. B **83**, 205101 (2011).
[9] C. K. Chan, P. A. Lee, K. S. Burch, J. H. Han, and Y. Ran, Phys. Rev. Lett. **116**, 1 (2016).
[10] M. N. Ali, J. Xiong, S. Flynn, J. Tao, Q. D. Gibson, L. M. Schoop, T. Liang, N. Haldolaarachchige, M. Hirschberger, N. P. Ong, and R. J. Cava, Nature **514**, 205 (2014).
[11] B. E. Brown, Acta Crystallogr. **20**, 268 (1966).
[12] Y. Zhang, J. van den Brink, C. Felser, and B. Yan, 2D Mater. **5**, 044001 (2018).
[13] L.-k. Shi and J. C. W. Song, Physical Review B **99**, 035403 (2019).
[14] Y. Zhang, Y. Sun, and B. Yan, Phys. Rev. B **97**, 041101 (2018).
[15] Q. Ma, S.-Y. Xu, H. Shen, D. MacNeill, V. Fatemi, T.-R. Chang, A. M. Mier Valdivia, S. Wu, Z. Du, C.-H. Hsu, S. Fang, Q. D. Gibson, K. Watanabe, T. Taniguchi, R. J. Cava, E. Kaxiras, H.-Z. Lu, H. Lin, L. Fu, N. Gedik, and P. Jarillo-Herrero, Nature **565**, 337 (2019).
[16] K. Kang, T. Li, E. Sohn, J. Shan, and K. F. Mak, Nature Materials **18**, 324 (2019).
[17] W. Yao, D. Xiao, and Q. Niu, Phys. Rev. B **77**, 235406 (2008).
[18] Y. M. Dai, J. Bowlan, H. Li, H. Miao, S. F. Wu, W. D. Kong, Y. G. Shi, S. A. Trugman, J. X. Zhu, H. Ding, A. J. Taylor, D. A. Yarotski, and R. P. Prasankumar, Phys. Rev. B **92**, 161104 (2015).
[19] Q. Wang, J. Li, J. Besbas, C.-H. Hsu, K. Cai, L. Yang, S. Cheng, Y. Wu, W. Zhang, K. Wang, T.-R. Chang, H. Lin, H. Chang, and H. Yang, Adv. Sci. **5**, 1700912 (2018).
[20] See Supplemental Material at [URL will be inserted by publisher] for Raman spectroscopy measurements and fitting procedures.

[21] F. Ye, J. Lee, J. Hu, Z. Mao, J. Wei, and P. X. Feng, Small **12**, 5802 (2016).
[22] K. Watanabe, T. Taniguchi, and H. Kanda, Nat. Mater. **3**, 404 (2004).
[23] Y. C. Jiang, J. Gao, and L. Wang, Sci. Rep. **6**, 19624 (2016).
[24] D. MacNeill, G. M. Stiehl, M. H. Guimaraes, R. A. Buhrman, J. Park, and D. C. Ralph, Nat. Phys. **13**, 300 (2017).
[25] P. Seifert, K. Vaklinova, S. Ganichev, K. Kern, M. Burghard, and A. W. Holleitner, Nat. Commun. **9**, 331 (2018).
[26] Q. Song, X. Pan, H. Wang, K. Zhang, Q. Tan, P. Li, Y. Wan, Y. Wang, X. Xu, M. Lin, X. Wan, F. Song, and L. Dai, Sci. Rep. **6**, 29254 (2016).
[27] M. Caputo, L. Khalil, E. Papalazarou, N. Nilforoushan, L. Perfetti, A. Taleb-Ibrahimi, Q. D. Gibson, R. J. Cava, and M. Marsi, Phys. Rev. B **97**, 115115 (2018).
[28] P. E. C. Ashby and J. P. Carbotte, Phys. Rev. B **89**, 245121 (2014).
[29] S. P. Mukherjee and J. P. Carbotte, Phys. Rev. B **96**, 085114 (2017).
[30] S. A. Yang, H. Pan, and F. Zhang, Phys. Rev. Lett. **115**, 156603 (2015).
[31] J. Lee, S. Sim, S. Park, C. In, S. Cho, S. Lee, S. Cha, S. Lee, H. Kim, J. Kim, W. Shim, J. S. Kim, D. Kim, and H. Choi, ACS Photonics **5**, 3347 (2018).
[32] Y. Liu, J. Besbas, Y. Wang, P. He, M. Chen, D. Zhu, Y. Wu, J. M. Lee, L. Wang, J. Moon, N. Koirala, S. Oh, and H. Yang, Nat. Commun. **9**, 2492 (2018).
[33] N. A. Sinitsyn, Q. Niu, J. Sinova, and K. Nomura, Phys. Rev. B **72**, 045346 (2005).
[34] S. Onoda, N. Sugimoto, and N. Nagaosa, Phys. Rev. Lett. **97**, 126602 (2006).
[35] J. C. W. Song and L. S. Levitov, Phys. Rev. B **90**, 075415 (2014).
[36] N. Nagaosa, J. Sinova, S. Onoda, A. H. MacDonald, and N. P. Ong, Rev. Mod. Phys. **82**, 1539 (2010).
[37] C. M. Yin, N. Tang, S. Zhang, J. X. Duan, F. J. Xu, J. Song, F. H. Mei, X. Q. Wang, B. Shen, Y. H. Chen, J. L. Yu, and H. Ma, Appl. Phys. Lett. **98**, 122104 (2011).
[38] J. W. McIver, B. Schulte, F. U. Stein, T. Matsuyama, G. Jotzu, G. Meier, and A. Cavalleri, arXiv preprint arXiv: 1811.03522 (2018).